JOURNAL OF APPLIED PHYSICS **106**, 103504 (2009)

A quality map of transfer printing

Matthew B. Tucker,[1] D. R. Hines,[2] and Teng Li[1,3,a)]
[1]*Department of Mechanical Engineering, University of Maryland, College Park, Maryland 20742, USA*
[2]*Laboratory for Physical Sciences, College Park, Maryland 20740, USA*
[3]*Maryland NanoCenter, University of Maryland, College Park, Maryland 20742, USA*

(Received 15 September 2009; accepted 16 October 2009; published online 17 November 2009)

Transfer printing is a nanofabrication technique that involves an assembly process by which a printable layer can be transferred from a transfer substrate to a device substrate. Future application of transfer printing toward a roll-to-roll printing process of flexible devices hinges upon the understanding on the mechanisms governing transfer printing quality, which is far from mature. So far, the quality control of transfer printing has been mainly explored via massive experimental trials, which are both time consuming and cost prohibitive. In this paper, we conduct systematic computational modeling to investigate the governing mechanisms of the transfer printing process. While the existing understanding of transfer printing mainly relies on the differential interfacial adhesion, our results suggest that both interfacial defects (e.g., cracks) and differential interfacial adhesion play pivotal roles in the transfer printing quality. The outcomes of this study define a quality map of transfer printing in the space spanned by the critical mechanical properties and geometrical parameters in a transfer printing structure. Such a quality map offers new insights and quantitative guidance for material selection and design strategies to achieve successful transfer printing. © *2009 American Institute of Physics*. [doi:10.1063/1.3259422]

I. INTRODUCTION

Large area, flexible electronics have emerged in recent years with an exciting array of potential applications,[1–4] ranging from paperlike displays[3] and skinlike smart prosthesis[5–7] to printable thin-film solar cells.[8,9] Future success of this promising technology relies on the reduced cost and enhanced reliability of flexible electronic devices. These attributes will come from new choices for materials and fabrication processes. For example, thin films of inorganic electronic materials (metals, Si, SiO_2, etc.) can be fabricated on compliant organic substrates (polymers, elastomers), resulting in lightweight, rugged, flexible devices.[10–12] Current microelectronics manufacturing processes require expensive fabrication facilities and are not scalable to large areas. The high temperature in certain processing steps is detrimental for the organic materials in flexible devices. Therefore, it is highly desirable to develop new fabrication technologies that are cost effective, scalable to large areas, and compatible with both organic materials and inorganic electronic materials. Transfer printing emerges as a potential fabrication technique to enable a low-cost and scalable roll-to-roll printing process of flexible devices.[13–19] Although transfer printing has been demonstrated in a wide range of material systems, the quality control of transfer printing has been mainly explored via massive experimental trials,[16,20] which are both time consuming and cost prohibitive, and thus lead to limited understanding. Aiming at a thorough understanding of the mechanisms governing transfer printing quality, this paper reports a comprehensive study of the effects of interfacial defects and device substrate stiffness on transfer printing, via computational modeling. The outcome of this study is a quality map of transfer printing, which can offer vital guidance for the structural design, defect control, and materials selection of flexible devices to be fabricated via transfer printing.

Transfer printing involves the transfer of a printable layer from a transfer substrate to a device substrate, and typically consists of two steps (Fig. 1).

(1) A transfer substrate (often a Si wafer is used for proof-of-concept work) containing a thin film of printable material is placed onto a device substrate (often a polymer or an elastomer), with the printable layer sandwiched between the two substrates. A pressure is applied along with an optional increase in temperature. For a thermoplastic polymer device substrate, it has been common to employ a temperature near or above the glass transition temperature of the device substrate material.

(2) The system is then cooled down to room temperature. The pressure is released and the transfer substrate is lifted from the device substrate. If the printable layer adheres more strongly to the device substrate than to the transfer substrate, the printable layer is left on the device substrate.

These two steps can be repeated to achieve multiple layer printing. Various organic and inorganic materials can be transfer printed in the same manner, thus avoiding mixed processing methods and allowing multilayer registration. Transfer printing is potentially an inexpensive process, scalable to continuous processing and does not rely on chemical processing. Unlike inkjet printing[21–25] and microcontact printing,[26–28] the transfer printing is inherently compatible with nanoscale features and the resulting devices are as good as those fabricated via traditional processing methods.[16]

In practice, a transfer printing process can result in successful, unsuccessful, or partial transfer printing of the printable layer onto the device substrate [Fig. 1(b)].[20] The under-

[a)]Author to whom correspondence should be addressed. Electronic mail: lit@umd.edu. Tel.: 301-405-0364. FAX: 301-314-9477.

 © 2009 American Institute of Physics

Downloaded 17 Nov 2009 to 129.2.19.102. Redistribution subject to AIP license or copyright; see http://jap.aip.org/jap/copyright.jsp

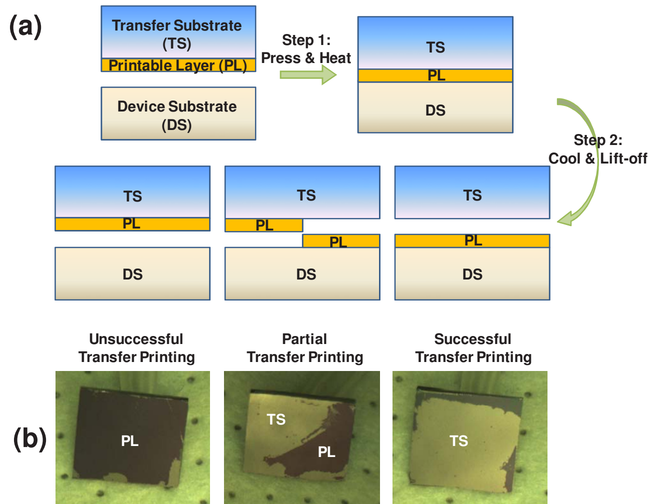

FIG. 1. (Color online) (a) Schematic of a transfer printing process that consists of two steps: (1) A printable layer is sandwiched between a transfer substrate and a device substrate under pressure and elevated temperature. (2) The structure is cooled and the transfer substrate is lifted off. After such a process, the printable layer can be either successfully transferred, or partially transferred, or unsuccessfully transferred onto the device substrate. (b) (From right to left) Optical images of silicon transfer substrates (bright region) and remaining printable layer of poly(methyl methacrylate) (PMMA) (dark region) after successful, partially successful, and unsuccessful transfer printing onto a poly(ethyleneterephthalate) (PET) device substrate, respectively. The percentage areas of PMMA layer transferred onto the PET substrate are 95%, 67%, and 5%, respectively, in these three cases. The size of the silicon transfer substrates is roughly 1×1 cm^2. The thicknesses of the PMMA layer and the PET device substrate are approximately 600 nm and 150 μm, respectively. In the successful case, the surfaces of both the printable layer and the device substrate were O_2 plasma-treated to improve adhesion; in the partial transfer printing case, only the device substrate surface was O_2 plasma treated, while in the unsuccessful case, no surface treatment was applied.

standing of critical transfer printing conditions governing print quality is still preliminary. For example, enhanced interfacial adhesion between the printable layer and the device substrate through plasma treatment[20] or applying a self-assembled adhesive monolayer[29] can lead to improved transfer printing quality. Further experiments have shown that the printing quality is also sensitive to both the specific geometry of the printable layer and the mechanical properties of organic/inorganic hybrid materials in the transfer printing structure, with quantitative dependence remaining elusive.

A successful transfer printing is essentially a well-controlled interfacial delamination process along the interface between the transfer substrate and the printable layer instead of that between the printable layer and the device substrate. During transfer printing, initial interfacial defects (e.g., cracks and voids) are highly likely to exist along the two interfaces in the trilayer structure. Such interfacial defects may result from unmatched surface roughness or uneven registration when printing over large areas. During the lift-off step, the interfacial defects, especially those near the edges, cause stress concentration and may lead to unstable interfacial delamination. Therefore, the initial interfacial defects can have pivotal impacts on the transfer printing quality. These impacts could be detrimental if the interfacial defects are along the interface between the printable layer and the device substrate (hereafter referred to as "the bottom interface"), but also could be beneficial if the interfacial defects are along the interface between the transfer substrate and the printable layer (hereafter referred to as "the top interface"). In practice, initial interfacial defects exist along both interfaces; therefore, it is the competition between the above two opposing impacts that crucially determines the transfer printing quality. So far little effort, if any, has been placed on the effect of competing interfacial delamination on transfer printing quality.[15,30]

Earlier studies have shown that substrate stiffness can substantially influence the driving force of the film-substrate interfacial delamination.[31–37] Most existing studies, however, dealt with the interfacial delamination in a film-on-substrate bilayer. The knowledge from these existing studies can shed light on, but is still insufficient for understanding the competing delamination along the two interfaces in the trilayer transfer printing structure. In particular, while a common proof-of-concept transfer substrate has often been made of silicon which is stiff, the device substrate material can range from modestly compliant polymers [e.g., poly(ethyleneterephthalate) (PET) and polyimide] to extremely compliant rubberlike elastomers [e.g., polydimethylsiloxane (PDMS)]. The wide range of device substrate stiffness (e.g., from 10 GPa to 1 MPa) and the huge stiffness ratio between the transfer substrate and the device substrate (e.g., from 10 to 10^5) can lead to rich characteristics of the competing delamination, which are far from well understood.

The lack of a thorough understanding of the science underpinning transfer printing quality poses a significant challenge for further developing transfer printing into a roll-to-roll process to fabricate flexible devices. To solve this challenge solely by experimental endeavors needs massive trials which are both time consuming and cost prohibitive. In this paper, using computational modeling, we conduct comprehensive parametric studies to quantitatively determine the effects of initial interfacial defects and device substrate stiffness, which result in a quality map of transfer printing that can be used to guide the structural design, defect control, and materials selection in flexible device fabrication. The rest of this paper is organized as follows. Section II describes the computational model; Sec. III reports the driving force for interfacial delamination along the two interfaces for various initial interfacial crack length combinations and various device substrate stiffnesses, from which the competing interfacial delamination is analyzed. A quality map of transfer printing emerges from further parametric studies and is reported in Sec. IV; concluding remarks are given in Sec. V.

II. COMPUTATIONAL MODEL

To study the effect of initial interfacial defects on the competing delamination in the trilayer structure of transfer printing, we use the finite element code ABAQUS to simulate the lift-off step of the transfer printing process. We focus on the impact of the initial interfacial cracks at the edges of the two interfaces in the trilayer structure. An edge crack results in higher driving force for interfacial delamination than that due to an interfacial crack of the same size embedded inside, and thus is more crucial in the transfer printing process. Dur-

Downloaded 17 Nov 2009 to 129.2.19.102. Redistribution subject to AIP license or copyright; see http://jap.aip.org/jap/copyright.jsp

ing lift-off, the mechanical separation causes opening displacement of both interfacial edge cracks. The driving force that causes the interfacial crack at the top interface (or bottom interface) to propagate is quantified by an energy release rate at the crack tip G_t (or G_b). If the driving force for the top interfacial crack, G_t, is greater than the interfacial adhesion energy between the transfer substrate and the printable layer, G_t^c, delamination along the top interface occurs. Similarly, if G_b is greater than the interfacial adhesion energy between the printable layer and the device substrate, G_b^c, delamination along the bottom interface occurs. Given that, in practice, the lift-off step is not loading-controlled, the competing delamination is thus governed by the *differential* driving force for crack propagation along the two interfaces, rather than their absolute values. That is, for a given combination of the interfacial adhesion energies in a transfer printing structure (i.e., G_t^c and G_b^c), if

$$G_t/G_b > G_t^c/G_b^c, \tag{1}$$

the top interfacial crack will propagate and initiate the delamination along the top interface. Alternatively, if

$$G_t/G_b < G_t^c/G_b^c, \tag{2}$$

the bottom interfacial crack will propagate and initiate the delamination along the bottom interface. In Eqs. (1) and (2), the left-hand side denotes the external driving force for delamination, and the right-hand side represents the intrinsic material resistance of the transfer printing structure to delamination. As will be shown later, once a delamination starts to propagate along an interface, the driving force keeps increasing as the crack advances, leading to a steady delamination along that interface until final separation. Therefore, the transfer printing quality can be characterized by the differential driving force of interfacial delamination in the following way:

$$G_t/G_b > G_t^c/G_b^c \rightarrow \text{successful transfer printing}$$

and

$$G_t/G_b < G_t^c/G_b^c \rightarrow \text{unsuccessful transfer printing}.$$

For example, for a transfer printing structure with equal interfacial adhesion energies ($G_t^c/G_b^c=1$), the transfer printing will be successful if $G_t/G_b>1$, and otherwise unsuccessful if $G_t/G_b<1$. In practice, a steady delamination along one interface could give its way to the fracture of the printable layer itself and the subsequent delamination along another interface, leading to the partial transfer printing. The fracture of the printable layer may result from the stress concentration near its own initial imperfections (e.g., microvoids and microcracks). The study of partially successful transfer printing is beyond the scope of this paper and will be further discussed in Sec. IV.

Figure 2(a) depicts the model used in the finite element simulations. We consider the transfer printing of a thin blanket printable layer; thus the trilayer structure is taken to deform under the plane strain conditions. In the finite element model, the thin printable layer is a film of thickness h, and both the transfer substrate and the device substrate are blocks of thickness $1000h$ and length $1000h$. Interfacial cracks of

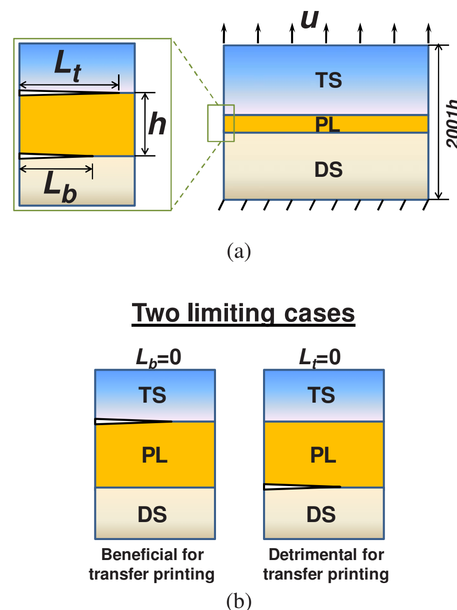

FIG. 2. (Color online) (a) Schematic of the computational model (not in scale). (b) Two limiting cases of interfacial cracks: one is beneficial for transfer printing ($L_t/h\neq 0$, $L_b/h=0$), and another is detrimental for transfer printing ($L_b/h\neq 0$, $L_t/h=0$).

length L_t and L_b are introduced at the left edge of the top and bottom interfaces in the trilayer structure, respectively. In simulations, L_t and L_b are varied to study the effect of the initial interfacial defect size. In a real transfer printing process, the thickness of the printable layer is about 100 nm, and that of the transfer substrate or device substrate is on the order of 100 μm. The vertical displacement is set to be zero along the bottom surface of the device substrate and set to be u along the top surface of the transfer substrate. This simulates the lift-off step of the transfer printing process. The quantity $\varepsilon=u/2001h$ will be called the applied strain. In a square region of $2h\times 2h$ near the tip of each interfacial crack, both the film and the portion of the corresponding substrate are densely meshed into four-node quadrilateral plane strain elements with an average element size of about $h/20$. The film and the substrate portions outside of these two square regions are meshed with triangle plane strain elements of matching sizes near the regions and coarser elements far away from the regions to reduce the computation time.

The transfer substrate, the printable layer, and the device substrate are modeled as isotropic elastic solids, which can be characterized by their Young's modulus E and Poisson's ratio ν. In the simulations, Young's modulus and Poisson's ratio of the transfer substrate are E_{TS}=71 GPa and ν_{TS}=0.16, respectively, and those of the printable layer are E_{PL}=78 GPa and ν_{PL}=0.44, respectively. These values are representative of a silicon transfer substrate and a thin-film gold printable layer. The mechanical properties of the device substrate (i.e., E_{DS} and V_{DS}) are varied to study their effect on the transfer printing quality. In the simulations, E_{DS}=2.6 GPa, 100 MPa, 10 MPa, 1 MPa and V_{DS}=0.37, 0.5, 0.5, 0.5 are used, respectively. These values are representative of a stiff polymer (e.g., PET) and three types of elas-

Downloaded 17 Nov 2009 to 129.2.19.102. Redistribution subject to AIP license or copyright; see http://jap.aip.org/jap/copyright.jsp

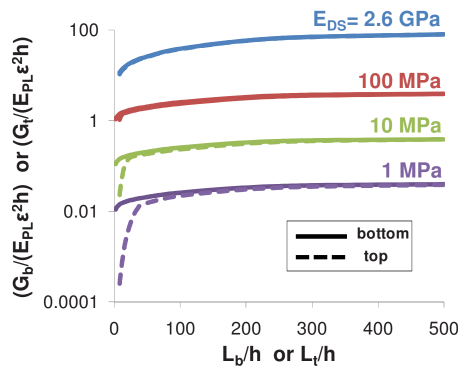

FIG. 3. (Color online) Solid lines: normalized energy release rate $G_b/E_{PL}\varepsilon^2h$ of an edge crack at the bottom interface as a function of normalized crack length L_b/h, for various device substrate stiffnesses. No crack exists at the top interface, corresponding to the detrimental limiting case in Fig. 2; Dashed lines: $G_t/E_{PL}\varepsilon^2h$ as a function of L_t/h for an edge crack at the top interface, for various device substrate stiffness. No crack exists at the bottom interface, corresponding to the beneficial limiting case in Fig. 2.

tomers (e.g., PDMS) of decreasing stiffness, respectively. The energy release rates of the two interfacial cracks are calculated by the contour integral in the finite element code ABAQUS. In describing the simulation results, we will use the following dimensionless groups: $G_t/E_{PL}\varepsilon^2h$, $G_b/E_{PL}\varepsilon^2h$, G_t/G_b, L_t/h, and L_b/h, which denote the normalized driving force of delamination along the top interface, the normalized driving force of delamination along the bottom interface, the differential driving force of delamination, the normalized length of the top interfacial crack, and the normalized length of the bottom interfacial crack, respectively.

III. RESULTS

We first consider two limiting cases, where an interfacial edge crack exists only at one of the two interfaces of a transfer printing structure, as illustrated in Fig. 2(b).

Figure 3 plots the normalized energy release rate $G_b/E_{PL}\varepsilon^2h$ (or $G_t/E_{PL}\varepsilon^2h$) of an edge crack along the bottom (or top) interface as a function of normalized crack length L_b/h (or L_t/h) for various device substrate parameters. In the first case (solid lines), there is no delamination allowed at the top interface, that is, $L_t/h=0$ (the printable layer is forced to transfer print). In the second case (dashed lines), there is no delamination allowed at the bottom interface, that is, $L_b/h=0$ (the printable layer is forced not to transfer print). In both cases, for given device substrate parameters (i.e., E_{DS} and ν_{DS}), the energy release rate at the interfacial crack tip increases monotonically as the crack length increases and saturates when the crack length reaches a value several hundred times greater than the thickness of the printable layer. As the device substrate stiffness decreases, the energy release rate drops considerably. This can be understood as follows. For a given applied strain ε as defined in Fig. 2, the more compliant the device substrate (i.e., smaller E_{DS}), the more applied strain is accommodated by the bulk deformation of the device substrate, thus the smaller the resulting driving force for the interfacial crack propagation. A comparison between the two limiting cases shows that, if the device substrate is sufficiently stiff (e.g., $E_{DS}>100$ MPa), the difference between the energy release rate of a top interfacial crack and that of a bottom interfacial crack of the same length is negligible. However, if the device substrate is compliant (e.g., $E_{DS}=10$ MPa or 1 MPa), the energy release rate of a top interfacial crack is much smaller than that of a bottom interfacial crack of the same length when the crack is short [e.g., L_t/h (or L_b/h) <20]. The difference diminishes and becomes negligible when the crack is significantly long [e.g., L_t/h (or L_b/h) >100]. Such a trend can also be explained by the more deformation accommodated by the bulk device substrate as its stiffness decreases. For an extremely compliant device substrate (e.g., $E_{DS}=1$ MPa), most of the applied strain is accommodated by the bulk device substrate, while the tranfer substrate and the printable layer deform little, leading to an extremely small energy release rate of a short interfacial crack along the top interface.

We next consider the more realistic condition where the printable layer is allowed to simultaneously delaminate from both substrates. This allows competing interfacial delamination during lift-off by determining the driving force for the propagation of interfacial edge cracks of various lengths along the two interfaces in a transfer printing structure. Given the monotonic increase in the energy release rate of the interfacial cracks with increasing crack length (as shown in Fig. 3), we focus hereafter on the competing interfacial delamination at the early stage of lift-off (i.e., smaller L_b/h and L_t/h with values <40).

Figure 4 plots the normalized energy release rates $G_b/E_{PL}\varepsilon^2h$ for an edge crack at the bottom interface and $G_t/E_{PL}\varepsilon^2h$ for an edge crack at the top interface as functions of the normalized bottom interfacial crack length L_b/h for various top interfacial crack lengths ($L_t/h=4,20,40$) and various device substrate parameters ($E_{DS}=2.6$ GPa, 100 MPa, 10 MPa, 1 MPa).

Take the case of $E_{DS}=2.6$ GPa as an example. For a given length of the edge crack at the top interface (e.g., $L_t/h=20$), the energy release rate of the bottom interfacial crack $G_b/E_{PL}\varepsilon^2h$ remains nearly zero while that of the top interfacial crack $G_t/E_{PL}\varepsilon^2h$ remains nearly a constant if the length of the bottom interfacial crack is much smaller than that of the top interfacial crack (i.e., $L_b/h \ll L_t/h$). As the lengths of the two interfacial cracks become comparable (i.e., $L_b/h \approx L_t/h$), the energy release rate of the bottom interfacial crack rapidly ramps up while that of the top interfacial crack abruptly drops down. When the bottom interfacial crack becomes slightly longer than the top interfacial crack (i.e., $L_b/h > L_t/h$), the energy release rate of the top interfacial crack becomes negligible while that of the bottom interfacial crack converges into the curve corresponding to $E_{DS}=2.6$ GPa in Fig. 3, no matter how long the top interfacial crack is. As the device substrate becomes more compliant (decreasing E_{DS}), the overall level of the energy release rates for both interfacial cracks decreases for a given applied strain ε, and the ramping up of $G_b/E_{PL}\varepsilon^2h$ and the dropping down of $G_t/E_{PL}\varepsilon^2h$ as L_b/h increases also become more gradual. The indication of the results shown in Fig. 4 on the transfer printing quality will be further elaborated in Fig. 6.

To further elucidate the interplay between the two interfacial cracks shown in Fig. 4, Fig. 5 plots the von Mises

Downloaded 17 Nov 2009 to 129.2.19.102. Redistribution subject to AIP license or copyright; see http://jap.aip.org/jap/copyright.jsp

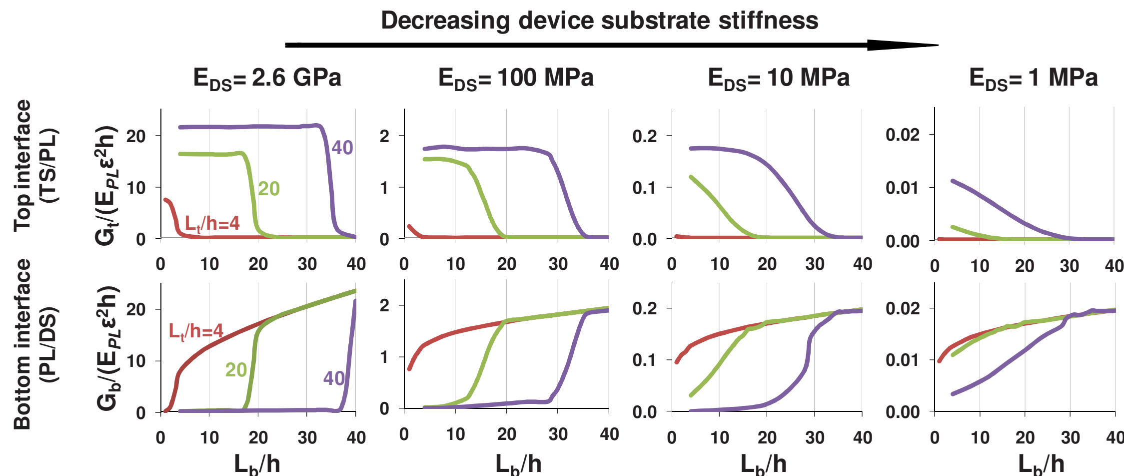

FIG. 4. (Color online) Normalized energy release rates $G_b/E_{PL}\varepsilon^2 h$ of an edge crack at the bottom interface and $G_t/E_{PL}\varepsilon^2 h$ of an edge crack at the top interface as functions of the normalized bottom interfacial crack length L_b/h for various top interfacial crack lengths L_t/h and device substrate stiffness E_{DS}.

stress field near the interfacial cracks for various crack length combinations (i.e., $L_t/h=20$ and $L_b/h=4,8,12,16,20$), under the same applied strain. Here $E_{DS}=2.6$ GPa (corresponding to the green lines in the leftmost plot of Fig. 4). The color shades in Fig. 5 represent the stress levels. For example, the uniform blue regions in the wake of the interfacial cracks indicate nearly zero stress level due to the free surface of the interfacial cracks. By contrast, the sharp transition from blue to red near the interfacial crack tip indicates significant stress concentration. As shown in Fig. 5, if $L_b/h \ll L_t/h$, the stress concentration only occurs near the tip of the top interfacial crack, while the low stress level near the tip of the bottom interfacial crack is comparable to that in the bulk substrates. As L_b/h increases (but is still smaller than L_t/h), the stress fields near the two crack tips remain approximately unchanged due to the shielding effect of the long top interfacial crack. When $L_b/h=L_t/h$, stress concentration occurs at both crack tips. If $L_b/h \gg L_t/h$ (not shown in Fig. 5), the top interfacial crack, in turn, is shielded by the longer bottom interfacial crack, leading to high stress concentration near the bottom crack tip but low stress level near the top crack tip.

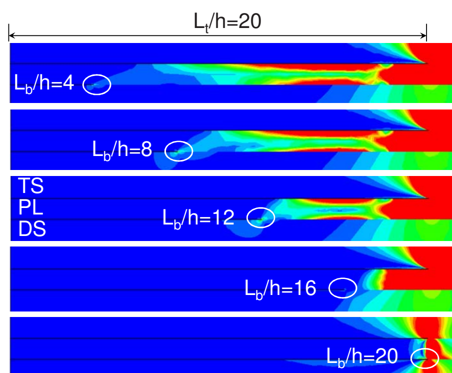

FIG. 5. (Color online) von Mises stress field near the interfacial cracks for various crack length combinations. Here $E_{DS}=2.6$ GPa, $L_t/h=20$. Color shades: red indicates high stress level and blue indicates low stress level. When $L_b/h < L_t/h$, the high stress concentration near the tip of the top interfacial crack remains approximately unchanged, while the stress level near the tip of the bottom interfacial crack is low. When $L_b/h=L_t/h$, stress concentration occurs at both crack tips. Note the maximum shielding effect of the top interfacial crack to the bottom interfacial crack when $L_b/h=16$.

Since the energy release rate scales with the square of the overall stress level near the crack tip, the trends in $G_b/E_{PL}\varepsilon^2 h$ and $G_t/E_{PL}\varepsilon^2 h$ as L_b/h and L_t/h vary, as shown in Fig. 4, can be readily understood.

IV. DISCUSSION

As described above, the transfer printing quality can be characterized by the differential driving force of interfacial delamination G_t/G_b, which can be deduced from the simulation results in Fig. 4. For example, Fig. 6 plots G_t/G_b as a function of L_b/h (with $L_t/h=20$, i.e., all green lines in Fig. 4) for various device substrate parameters. For a given combination of interfacial crack lengths (i.e., L_b/h and L_t/h), the differential driving force of interfacial delamination increases as the device substrate stiffness increases. The physical significance of Fig. 6 can be further explained as follows.

Take the case of equal interfacial adhesion energies ($G_t^c/G_b^c=1$) as an example. The $G_t/G_b-L_b/h$ curve for $E_{DS}=2.6$ GPa crosses the line of $G_t/G_b=1$ at $L_b/h=18.9$. [The spike in the $G_t/G_b-L_b/h$ curve for $E_{DS}=2.6$ GPa occurs at $L_b/h=16$, where the shielding of the long top interfacial crack to the bottom one maximizes, resulting in a much smaller G_b. This is evident in Fig. 5 which clearly shows the much reduced stress level near the tip of the bottom interfacial crack when $L_b/h=16$, while the stress concentration near

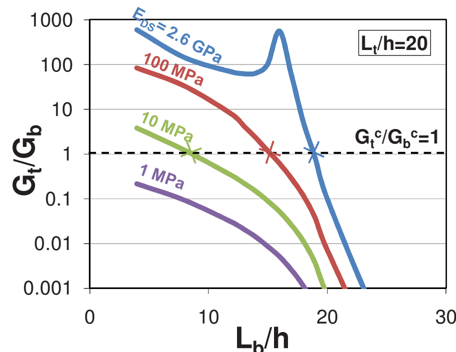

FIG. 6. (Color online) G_t/G_b as a function of L_b/h for various device substrates. Here $L_t/h=20$. The dashed line denotes the case of equal interfacial adhesion energy $G_t^c/G_b^c=1$.

Downloaded 17 Nov 2009 to 129.2.19.102. Redistribution subject to AIP license or copyright; see http://jap.aip.org/jap/copyright.jsp

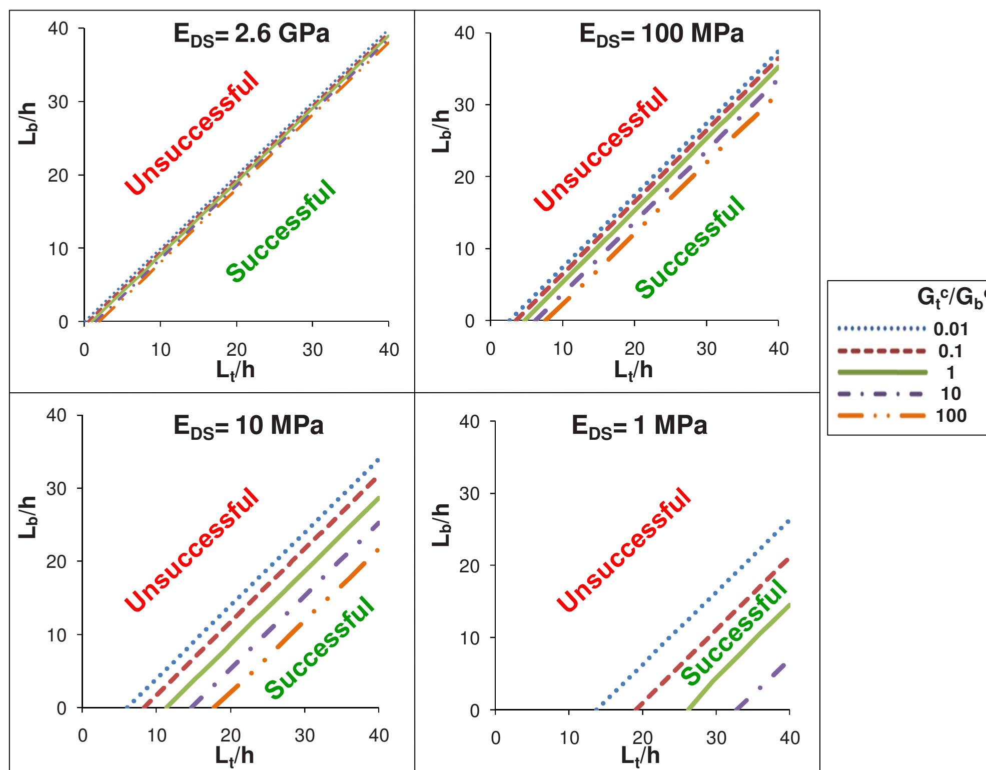

FIG. 7. (Color online) A quality map of transfer printing. Each curve defines a boundary line in the space of L_b/h and L_t/h, for a given E_{DS} and G_t^c/G_b^c, below which transfer printing is expected to be successful and otherwise unsuccessful.

the tip of the top crack remains roughly unchanged as L_b/h varies. Further simulations reveal that such a spike only exists when a stiff device substrate (e.g., E_{DS}=2.6 GPa) is used. For compliant device substrates (e.g., E_{DS}=100 MPa, 10 MPa, 1 MPa), G_t/G_b decreases monotonically as L_b/h increases.] That is, for a given edge crack of length 20h along the top interface, there is a critical length of an edge crack along the bottom interface L_b^c=18.9h, shorter than which transfer printing is successful (i.e., $G_t/G_b > G_t^c/G_b^c$) and longer than which transfer printing is unsuccessful (i.e., $G_t/G_b < G_t^c/G_b^c$). Similarly, for device substrates of intermediate stiffness, E_{DS}=100 MPa and 10 MPa, the transition from successful to unsuccessful transfer printing occurs at L_b^c=15.3h and 8.5h respectively. Furthermore, on a very compliant device substrate (E_{DS}=1 MPa), transfer printing cannot be successful if the interfacial adhesion energies are equal and an edge crack of length 20h exists at the top interface.

In practice, the interfacial adhesion of the top and the bottom interfaces can be considerably different (e.g., plasma treatment of the bottom interface can lead to significant decrease in G_t^c/G_b^c). The values of L_b^c in those cases can be determined from Fig. 6 in the similar manner. For example, for E_{DS}=10 MPa, L_b^c increases from 8.5h to 14.8h if G_t^c/G_b^c decreases from 1 to 0.1; that is, an enhanced interfacial adhesion along the bottom interface results in a transfer printing process that is more tolerant of the defects at the bottom interface. The enhanced interfacial adhesion along the bottom interface (e.g., G_t^c/G_b^c=0.1) also allows successful transfer printing on a very compliant substrate (E_{DS}=1 MPa).

Progressing beyond Fig. 6 which illustrates a quantitative approach to determine the transfer printing quality, a comprehensive parametric study can be undertaken to define a *quality map* of transfer printing in the space spanned by device substrate stiffness, interfacial crack lengths, and interfacial adhesion energies of the two interfaces in a transfer printing structure. Such a quality map is depicted in Fig. 7.

For a given plot in Fig. 7 (i.e., a specific device substrate stiffness E_{DS}), each line corresponds to an order of magnitude change in the differential adhesion (ratio of the interfacial adhesion energies of the two interfaces G_t^c/G_b^c). Each line constitutes a boundary between which the transfer printing is expected to be either successful (below a line) or unsuccessful (above a line). That is, for a given top interfacial crack of length L_t/h, the boundary line defines a critical length of the bottom interfacial crack, smaller than which the interfacial delamination will propagate along the top interface, leading to a successful transfer printing process. Such a critical length increases as G_t^c/G_b^c decreases, that is, as the interfacial adhesion of the bottom interface becomes relatively stronger than that of the top interface, the transfer printing process is more tolerant of the defects at the bottom interface. When comparing various device substrate cases, for a given G_t^c/G_b^c, the successful transfer printing region defined by the boundary line in the space of $L_b/h-L_t/h$ becomes smaller as E_{DS} decreases. Therefore, a more compliant device substrate is less tolerant of the defect along the interface between the printable layer and the device substrate. Conceptually, it can be noted that, for a stiffer device substrate, large changes in the differential adhesion do not affect the ability to successfully transfer print as much as do changes in the interfacial crack lengths. This is evident by

Downloaded 17 Nov 2009 to 129.2.19.102. Redistribution subject to AIP license or copyright; see http://jap.aip.org/jap/copyright.jsp

the small separation between the boundary lines in the plot for $E_{DS}=2.6$ GPa. As the device substrate becomes more compliant, not only does successful transfer printing becomes harder (lines shifted to larger values of L_t/h) but also changes in the differential adhesion more strongly affect the ability to successfully transfer print the printable layer onto the device substrate. For a very compliant device substrate ($E_{DS}=1$ MPa), even with an adhesion to the device substrate 100 times greater than the adhesion to the transfer substrate ($G_t^c/G_b^c=0.01$), transfer printing will not be successful without an initial top interface crack length of at least $14h$.

The significance and implication of the quality map of transfer printing depicted in Fig. 7 can be further delineated as follows.

(1) *The transfer printing quality is determined not only by the relative interfacial adhesion* G_t^c/G_b^c *in the trilayer transfer printing structure but also by the defects (e.g., cracks) along the two interfaces*. In certain cases, the transfer printing quality could even be dominated by the interplay between the interfacial defects. For example, for a stiff device substrate (e.g., $E_{DS}=2.6$ GPa), all boundary lines, ranging from $G_t^c/G_b^c=0.01$ to 100, are close to each other. In other words, even a huge difference in the relative interfacial adhesion leads to an insignificant change in the transfer printing quality. In contrast, the quality of transfer printing is rather dominated by the relative length of the interfacial cracks, when a stiff device substrate is used.

(2) *Transfer printing onto a compliant device substrate is more challenging than onto a stiff device substrate*. This is evident as the decreasing successful transfer printing region in the space of L_b/h and L_t/h as the device substrate becomes more compliant, as shown in Fig. 7. Such a prediction in general agrees with the experimental observations.[16] Also evident in Fig. 7 is that, for more compliant device substrates, the transfer printing quality can be more tailored by improving the interfacial adhesion along the bottom interface or worsening that along the top interface, as indicated by the increasing spacing between the boundary lines in the space of L_b/h and L_t/h for various G_t^c/G_b^c.

(3) *Transfer printing quality can be enhanced by controlling the interfacial defects*. All the boundary lines in Fig. 7 show a monotonic increase trend in the space of $L_b/h - L_t/h$, which suggests a practical strategy to improve the transfer printing quality by introducing initial defects along the top interface of a transfer printing structure. This can be achieved by controlled surface treatment of the transfer substrate in the regions to be registered to the edges of the printable layers. Figure 7 offers a quantitative guideline for the size of the top interfacial crack to be introduced to achieve a certain tolerance of the natural interfacial defects along the bottom interface in a transfer printing process. Alternatively, transfer printing quality can also be improved by reducing the size of possible interfacial defects along the bottom interface (e.g., via minimizing the surface roughness of the device substrate). In this regard, Fig. 7 sheds light on the desired device substrate surface roughness to control the interfacial crack size along the bottom interface. To the best of our knowledge, the above suggested strategies have not yet been experimentally explored in a systematic manner, and thus open up new pathways to enhance transfer printing quality.

The simulation model reported in this paper focuses on the lift-off step in a transfer printing process. In practice, the first step of transfer printing involves a heat-up/cool-down thermal cycle, which can potentially result in residual thermal stress in the transfer printing structure. More specifically, given the higher coefficients of thermal expansion for the polymer/elastomer materials ($100\ \mathrm{s}\times10^{-6}/{}^\circ\mathrm{C}$, i.e., device substrates) than those for metals and silicon ($\sim10\times10^{-6}/{}^\circ\mathrm{C}$, i.e., printable layers and transfer substrates), it is expected that the thermal mismatch stress along the bottom interface (with the printable layer in compression and the transfer substrate near the interface in tension) will be higher than that along the top interface. Such a higher thermal mismatch stress may lead to a larger driving force for the interfacial delamination along the bottom interface. Therefore, the residual thermal stress is expected to be detrimental for the transfer printing process. Nonetheless, such a negative impact is rather limited given the modest temperature range of the thermal cycle (e.g., $\sim100\ ^\circ\mathrm{C}$). Above said, the present study may slightly overestimate the transfer printing quality. In our model, we assume the plain strain deformation of the transfer printing structure during the lift-off. This assumption is reasonable if the feature size of the printable layer (i.e., width and length) is much larger than its thickness, which is generally justified. In practice, the transfer printing of small features with sharp corners (e.g., islands and vias) is also desirable. During the lift-off, the sharp corners cause higher stress concentration and may initiate the interfacial delamination in either or both interfaces. Studying the effect of the sharp corners of the printable layers on transfer printing quality requires simulations of the competing interfacial delamination in three dimensions, thus is not yet considered in the present model. In real transfer printing processes, it is also possible to have the printable layer partially transferred onto the device substrate [e.g., Fig. 1(b)]. Partial transfer printing may result from the initial defects (e.g., microvoids, microcracks, and nonuniform thickness) in the printable layer or pre-existing interfacial defects of abnormal sizes that can abruptly change the competing physics of the interfacial delamination. Further investigation on the impact of the abovementioned issues is necessary to reach a thorough understanding of the mechanisms underpinning transfer printing quality, which will be reported elsewhere in the future.

V. CONCLUDING REMARKS

This paper aims to explore the science underpinning the transfer printing process and thus identify the mechanisms governing transfer printing quality, through comprehensive computational modeling. The outcomes of this study define a quality map of transfer printing in the space spanned by the critical mechanical properties and geometrical parameters in a transfer printing structure. Some major findings emerging from the quality map are recapped as follows:

(1) While the existing understanding of transfer printing mainly relies on the differential interfacial adhesion,[16] the

Downloaded 17 Nov 2009 to 129.2.19.102. Redistribution subject to AIP license or copyright; see http://jap.aip.org/jap/copyright.jsp

results in this paper suggest that both interfacial defects (e.g., cracks) and differential interfacial adhesion play pivotal roles in transfer printing quality.

(2) Transfer printing onto a stiff device substrate is dominated by the interfacial defects and is less sensitive to the differential adhesion. In contrast, transfer printing onto a compliant device substrate, although more challenging, can be significantly improved by tailoring the differential interfacial adhesion.

(3) Controlling the interfacial defects offers new pathways to improve transfer printing quality which remain largely unexplored. The results in this paper provide quantitative guidance on interfacial defect control to achieve certain criteria of transfer printing quality.

In summary, the quality map of transfer printing reveals critical mechanical and geometrical parameters that govern the transfer printing process, and offer new insights toward optimal printing conditions. While such a quality map may potentially accelerate the advance and reduce the cost toward the maturation of transfer printing technology, we call for further systematic experimental validation and demonstration, which are crucial for paving the way to the application of transfer printing into a roll-to-roll printing process.

ACKNOWLEDGMENTS

This research is supported by National Science Foundation (under Grant Nos. 0856540 and 0928278) and Minta Martin Foundation.

[1]R. H. Reuss, B. R. Chalamala, A. Moussessian, M. G. Kane, A. Kumar, D. C. Zhang, J. A. Rogers, M. Hatalis, D. Temple, G. Moddel, B. J. Eliasson, M. J. Estes, J. Kunze, E. S. Handy, E. S. Harmon, D. B. Salzman, J. M. Woodall, M. A. Alam, J. Y. Murthy, S. C. Jacobsen, M. Olivier, D. Markus, P. M. Campbell, and E. Snow, Proc. IEEE **93**, 1239 (2005).
[2]A. Nathan and B. R. Chalamala, Proc. IEEE **93**, 1235 (2005).
[3]G. P. Crawford, *Flexible Flat Panel Displays* (Wiley, Chichester, 2005).
[4]S. Forrest, Nature (London) **428**, 911 (2004).
[5]T. Someya, T. Sekitani, S. Iba, Y. Kato, H. Kawaguchi, and T. Sakurai, Proc. Natl. Acad. Sci. U.S.A. **101**, 9966 (2004).
[6]T. Someya, Y. Kato, T. Sekitani, S. Iba, Y. Noguchi, Y. Murase, H. Kawaguchi, and T. Sakurai, Proc. Natl. Acad. Sci. U.S.A. **102**, 12321 (2005).
[7]S. Wagner, S. Lacour, J. Jones, P. Hsu, J. Sturm, T. Li, and Z. Suo, Physica E (Amsterdam) **25**, 326 (2004).
[8]G. Dennler and N. S. Sariciftci, Proc. IEEE **93**, 1429 (2005).
[9]C. J. Brabec, Sol. Energy Mater. Sol. Cells **83**, 273 (2004).
[10]K. Jain, M. Klosner, M. Zemel, and S. Raghunandan, Proc. IEEE **93**, 1500 (2005).
[11]R. Ludwig, R. Kukla, and E. Josephson, Proc. IEEE **93**, 1483 (2005).
[12]G. Abbie, L. York, and M. Strnad, in *Flexible Flat Panel Displays*, edited by G. P. Crawford (Wiley, New York, 2005).
[13]Y. G. Sun and J. A. Rogers, Nano Lett. **4**, 1953 (2004).
[14]D. R. Hines, S. Mezhenny, M. Breban, E. D. Williams, V. W. Ballarotto, G. Esen, A. Southard, and M. S. Fuhrer, Appl. Phys. Lett. **86**, 163101 (2005).
[15]M. A. Meitl, Z. T. Zhu, V. Kumar, K. J. Lee, X. Feng, Y. Y. Huang, I. Adesida, R. G. Nuzzo, and J. A. Rogers, Nature Mater. **5**, 33 (2006).
[16]D. R. Hines, V. W. Ballarotto, E. D. Williams, Y. Shao, and S. A. Solin, J. Appl. Phys. **101**, 024503 (2007).
[17]X. Liang, Z. Fu, and S. Y. Chou, Nano Lett. **7**, 3840 (2007).
[18]A. J. Tunnell, V. W. Ballarotto, D. R. Hines, and E. D. Williams, Appl. Phys. Lett. **93**, 193113 (2008).
[19]K. H. Yim, Z. J. Zheng, Z. Q. Liang, R. H. Friend, W. T. S. Huck, and J. S. Kim, Adv. Funct. Mater. **18**, 1012 (2008).
[20]D. Y. Lee, D. R. Hines, C. M. Stafford, C. L. Soles, E. K. Lin, and G. S. Oehrlein, Adv. Mater. (Weinheim, Ger.) **21**, 2524 (2009).
[21]H. Sirringhaus, T. Kawase, R. H. Friend, T. Shimoda, M. Inbasekaran, W. Wu, and E. P. Woo, Science **290**, 2123 (2000).
[22]P. Calvert, Chem. Mater. **13**, 3299 (2001).
[23]T. Kawase, H. Sirringhaus, R. H. Friend, and T. Shimoda, Adv. Mater. (Weinheim, Ger.) **13**, 1601 (2001).
[24]T. Kawase, T. Shimoda, C. Newsome, H. Sirringhaus, and R. H. Friend, Thin Solid Films **438–439**, 279 (2003).
[25]M. L. Chabinyc, W. S. Wong, A. C. Arias, S. Ready, R. A. Lujan, J. H. Daniel, B. Krusor, R. B. Apte, A. Salleo, and R. A. Street, Proc. IEEE **93**, 1491 (2005).
[26]A. Kumar and G. M. Whitesides, Appl. Phys. Lett. **63**, 2002 (1993).
[27]J. L. Wilbur, A. Kumar, E. Kim, and G. M. Whitesides, Adv. Mater. (Weinheim, Ger.) **6**, 600 (1994).
[28]Y. N. Xia, J. A. Rogers, K. E. Paul, and G. M. Whitesides, Chem. Rev. (Washington, D.C.) **99**, 1823 (1999).
[29]Y. L. Loo, R. L. Willett, K. W. Baldwin, and J. A. Rogers, J. Am. Chem. Soc. **124**, 7654 (2002).
[30]X. Feng, M. A. Meitl, A. M. Bowen, Y. Huang, R. G. Nuzzo, and J. A. Rogers, Langmuir **23**, 12555 (2007).
[31]S. L. Chiu, J. Leu, and P. S. Ho, J. Appl. Phys. **76**, 5136 (1994).
[32]H. H. Yu, M. Y. Ye, and J. W. Hutchinson, Acta Mater. **49**, 93 (2001).
[33]B. E. Alaca, M. T. A. Saif, and H. Sehitoglu, Acta Mater. **50**, 1197 (2002).
[34]T. Li, Z. Huang, Z. Xi, S. Lacour, S. Wagner, and Z. Suo, Mech. Mater. **37**, 261 (2005).
[35]N. S. Lu, J. I. Yoon, and Z. G. Suo, Int. J. Mater. Res. **98**, 717 (2007).
[36]T. Li and Z. Suo, Int. J. Solids Struct. **44**, 1696 (2007).
[37]H. X. Mei, R. Huang, J. Y. Chung, C. M. Stafford, and H. H. Yu, Appl. Phys. Lett. **90**, 151902 (2007).

Downloaded 17 Nov 2009 to 129.2.19.102. Redistribution subject to AIP license or copyright; see http://jap.aip.org/jap/copyright.jsp